J Mol Model (2009) 15:1317–1328
DOI 10.1007/s00894-009-0493-2

ORIGINAL PAPER

Structure and dynamics of the influenza A M2 Channel: a comparison of three structures

Hadas Leonov · Isaiah T. Arkin

Received: 5 January 2009 / Accepted: 19 February 2009 / Published online: 18 April 2009

Abstract The M2 protein is an essential component of the Influenza virus' infectivity cycle. It is a homo-tetrameric bundle forming a pH-gated H^+ channel. The structure of M2 was solved by three different groups, using different techniques, protein sequences and pH environment. For example, solid-state NMR spectroscopy was used on a protein in lipid bilayers, while X-ray crystallography and solution NMR spectroscopy were applied on a protein in detergent micelles. The resulting structures from the above efforts are rather distinct. Herein, we examine the different structures under uniform conditions such as a lipid bilayer and specified protonation state. We employ extensive molecular dynamics simulations, in several protonation states, representing both closed and open forms of the channel. Exploring the properties of each of these structures has shown that the X-ray structure is more stable than the other structures according to various criteria, although its water conductance and water-wire formation do not correlate to the protonation state of the channel.

Keywords Influenza · Ion channel · Molecular dynamics · Protein structure

Introduction

M2, a critical component of the influenza virus, is a 97-residue, bitopic membrane protein that plays a vital role in the viral entry process via endocytotic uptake. M2 has an amino termini that protrudes into the exterior of the virus, while the carboxy termini resides in the viral lumen. The transmembrane region forms a homotetrameric helical bundle that functions as a pH-activated H^+ channel [1, 2]. Acidification of the endosome leads to the activation of M2, thus opening the channel and allowing protons to pass from the endosome into the virus interior. This, in turn, leads to acidification of the virus interior and the release of the viral RNA into the host's cytoplasm, which is eventually transported into the nucleus and replicated to create new virions. The replication of the influenza A virus can be stopped by inhibiting the activity of the M2 channel. One such inhibitor is the hydrophobic anti-influenza drug, amantadine. However, mutations in M2 at residues Val-27, Ala-30 and Ser-31 result in amantadine-resistant viral strains, most notably S31N [3–5].

The pH activation of M2 is attributed to the four His-37 residues located in the channel pore [6]. M2 is impermeable to sodium and potassium ions, and is highly selective for protons [7–10]. M2 was shown to be a low conductance channel, measured in units of aS [10]. A more recent study presented single channel proton conductivity measurements of 6 pS [11], that are higher by several orders of magnitude than the previous estimate [10]. The reason for the difference may stem from the lower pH used in the latter research, since single channel proton conductance can only be measured at a high concentration of H^+, as well as different lipids and conditions that do not disrupt the protein's structure at a low pH.

Two mechanisms of conductance were suggested for the channel: gating [12] and shuttling [2]. In the gating mechanism, conductivity is achieved when water molecules are able to penetrate the pore while forming a continuous proton wire [13]. The gating itself is theorized to be con-

H. Leonov · I. T. Arkin (✉)
Department of Biological Chemistry,
The Alexander Silberman Institute of Life Sciences,
The Hebrew University of Jerusalem,
Edmund J. Safra Campus Givat-Ram,
Jerusalem 91904, Israel
e-mail: arkin@huji.ac.il

trolled by the His-37 residues when the pH is low (~5.5–6.0) due to protonation and repulsion of the Histidine side chains. In the shuttling mechanism, the histidines are directly involved in the proton transfer mechanism through tautomerization or a ring flip of the histidines [14].

Various modeling and computational studies were performed on M2, trying to determine its structure and mechanism of action. The first computations were performed in vacuo [12, 15], followed by studies in lipid bilayers [16–19]. An experimentally derived structure of M2 based on solid-state NMR data (ss-NMR) was published in 2002 [20], and presented some differences from the previous models. The theoretical models predicted helix tilt angles of 10°–15°, a much lower range than that determined experimentally: 32°–38° [21, 22]. Later on, simulations based on the ss-NMR structure have emerged, examining rotamers for open and closed forms [23], exploring the correlation of different protonation states of the His-37 residue to the pore's structure [24] and investigating the ion selectivity, amantadine binding and proton transport in different protonation states [25].

Recently, two more experimental structures of M2 have emerged (both in detergent micelles): an X-ray structure by DeGrado and colleagues [26], and a solution NMR structure by Chou and colleagues [27]. The X-ray study produced two structures: an I33-SeMet mutant at pH 7.3 at a resolution of 2.05Å, and an amantadine-bound complex of the G34A mutant at pH 5.3 at a resolution of 3.5Å. The crystal structure of both amantadine bound and unbound forms were remarkably similar (Cα-RMSD of 1.1Å) and were shaped like a truncated cone which is narrow at the N-terminal facing the exterior. The helices are tilted by ~35° from the bundle axes. The structure shows that the channel is most constricted around Val-27 (2.7Å) and opens until a maximal diameter of 9Å near Gly-34. The structural properties of a single helix from the X-ray structure and the solid state NMR structure [28] are nearly the same, however the tetramer complex is very different.

The solution NMR structure [27] is claimed by the authors to be more reliable and stable than previous computational and experimental models because it was determined with an extra C-terminal region which other models lack. The helical bundle derived from the latter NMR structure is yet again different from the two previously published structures (see Fig. 1), so it is unclear which structure is most similar to the native structure of the real M2 channel. In summary, the Cα-RMSD differences between the different structures in the transmembrane (TM) region are: (i) X-ray versus ssNMR: 13.8Å; (ii) X-ray versus solution NMR: 4.0Å and (iii) ssNMR versus solution NMR: 12.8Å.

Taken together, one is confronted with three experimental structures for the M2 channel that were obtained under different conditions (e.g., bilayer versus detergent micelle, pH) using different methodologies. Therefore, the aim of this study was to compare the three different structures by way of analyzing their dynamics under uniform conditions such as a lipid bilayer and specified protonation state.

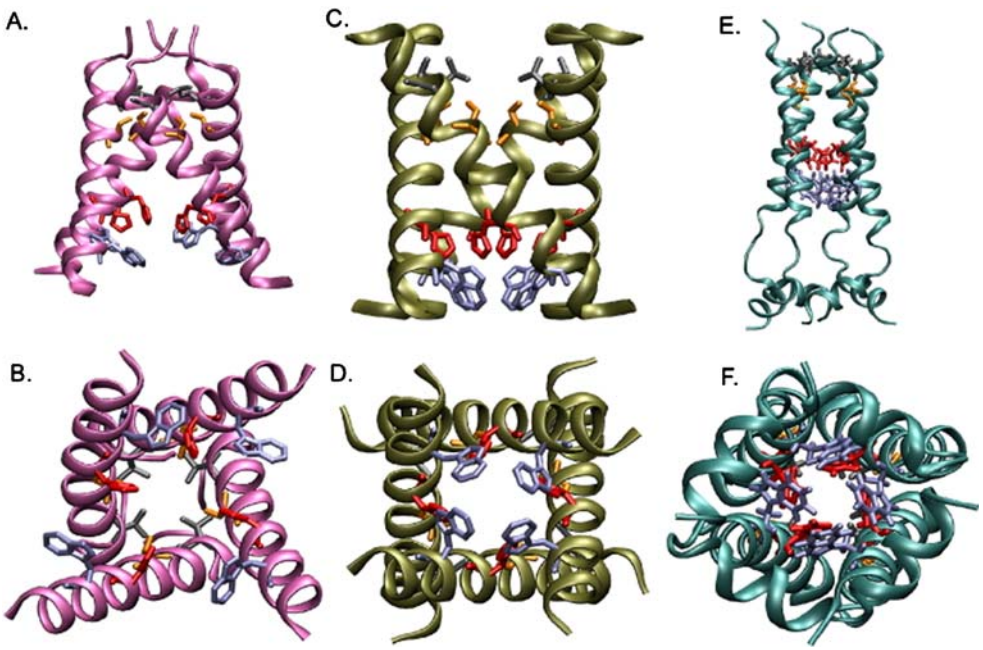

Fig. 1 Schematic diagrams of the three experimental structures of the M2 H+ channel from Influenza A in a view from the side and top. (**A**)–(**B**) derive from DeGrado's X-ray structure [26], (**C**)–(**D**) derive from Cross' solid state NMR [28], (**E**)–(**F**) derive from Chou's solution NMR [27]. The Histidine residues are shown in red, Serine in orange, Valine in gray and Tryptophan in light blue

Materials and methods

Initial structures

The initial structures used in this study were derived from three experimental structures: (i) X-ray structure in octyl-β-D-glucopyranoside micelles solved at pH 7.3, PDB code: 3BKD [26]. (ii) Structure derived from ss-NMR data obtained in DMPC lipid bilayer and pH 7, PDB code: 1NYJ [20] (iii) Solution NMR data in 1,2-diheptanoyl-sn-glycero-3-phosphocholine detergent micelles at pH 7.5, PDB code: 2RLF [27].

Simulation setup

The protein was embedded in a pre-equilibrated dimyristoylphosphocholine (DMPC) bilayer downloaded from Peter Tieleman's website[1]. The bilayers initially contained 128 lipids embedded in 3687 molecules of SPC water [29]. The DMPC force-field parameters were taken from [33]. The principal axis of the helical bundle of each of the initial structures was aligned to the bilayer normal and colliding lipids were removed in range of 1–1.5 Å from the protein. After the automatic removal of lipids, a visual inspection was performed, and lipids that clashed with the structure were manually removed. The X-ray structure preparation included two additional stages. (i) The original PDB contained crystal water molecules that were kept during the simulation. However, they appeared only as oxygen atoms, therefore, hydrogen atoms were added. (ii) The original PDB contained a residue of Selenomethionine that was changed to Methionine.

For each structure, a few protonation states of the His-37 were examined: 0 (neutral), +2 (bi-protonated), +3 (tri-protonated). A neutral channel in which no histidines are charged is expected to be closed, while, a +3 protonation state should mimic an open channel [30]. A +2 state represents an intermediate protonation state that had been proposed to be conductive as well [24]. Finally, in order to neutralize the system's charge for the electrostatic calculations, Na^+ counter ions randomly replaced water molecules in the system. The number of counter ions was determined according to the overall charge of the channel, which changed according to the protonation state of His-37. The neutral, bi-protonated and tri-protonated systems contained 4, 2 and 1 Na^+ counter ions respectively. The details of each system are specified in Table 1. It can be seen that the major differences between the systems are the number of protein residues and number of water molecules. For the X-ray and ssNMR structures, there are 25 residues per helix, thereby making a total of a 100 residues. For the solution NMR structure that includes a longer C-terminal tail, there are 38 residues per helix and 152 protein residues in total. Water molecules were added to the last system in order to solvate the whole protein.

[1] http://moose.bio.ucalgary.ca/index.php?page=Structures_and_Topologies

Simulation steps

Energy minimization

Each system underwent energy-minimization with the steepest descent algorithm with a tolerance of 300 kJ mol^{-1} nm^{-1}. In the X-ray structure, the crystal waters were positionally restrained during the minimization, in order to retain their original location.

Positional restraints

In order to prevent high perturbations when moving from the positional restrained system to unrestrained molecular dynamics where the atoms move freely, we have used a gradual positional restraints (PR) procedure, in which the force constant constraining the protein and lipid atoms was gradually decreased from 1000 to 0 kJ mol^{-1} nm^{-2}. When the constraints lessen, the molecules move more freely and may need longer equilibration time. For that reason, the procedure began by restraining the atoms using a harmonic restraint, with a force constant of k=1000 kJ mol^{-1} nm^{-2} for 20 ps. Subsequent PR steps were run with a lower force constant while linearly increasing the simulation time to 100 ps at k=0 kJ mol^{-1} nm^{-2}. Furthermore, the force constant was decreased by a smaller step size when the force became less stringent, starting with a step size of dk=10 (1000, 990, 980 . . .), continuing with a step of dk=5 around k=200 kJ mol^{-1} nm^{-2} and decreasing to dk=1 from k=100 . . . 0 kJ mol^{-1} nm^{-2}. The exact cutoffs in which the step size changed were different for each PR, according to the system stability. The total time of the positional restraints process was around 10–15 ns for each structure.

MD simulations

The systems were subjected to 2–3 trials of a 20 ns molecular dynamics (MD) simulation in order to test their convergence (see Table 1). The simulations were conducted using version 3.3.1 of the GROMACS MD simulation package [31] employing an extended version of the united atoms GROMOS87 force field [32].

All simulations were conducted using the LINCS algorithm [34] to constrain bond lengths and angles of hydrogen atoms, allowing for an integration time step of

Table 1 Summary of MD simulations

Structure	Protonation state	Residues number	Lipids number	Water mol. number	Number of trials	Total time (ns)
X-ray (pdb: 3BKD)	0-H	100	101	3661	3	60
X-ray	2-Hs	100	101	3663	3	60
X-ray	3-H	100	101	3663	3	60
ssNMR (pdb: 1NYJ)	0-H	100	93	3603	2	40
ssNMR	2-Hs	100	92	3605	2	40
ssNMR	3-H	100	93	3606	2	40
solution NMR (pdb: 2RLF)	0-H	152	98	4645	2	40
solution NMR	2-Hs	152	98	4642	2	40
solution NMR	3-H	152	98	4641	2	40

The terms 0-H, 2-Hs, 3-H refer to the protonation state of M2: neutral, symmetrically bi-protonated, and tri-protonated, respectively. The number of molecules for each section of the system is listed as well. Trials of the same system may contain minor differences in lipid and water molecules number due to clashes.

2 fs. Atomic coordinates were saved every 10 ps. Simulations were conducted at a constant temperature of 310 K. Solvent, lipids, and protein were coupled separately to a Nose-Hoover temperature bath [35, 36], with a coupling constant of τ=3 ps. The pressure was kept constant by a semi-isotropic, Parrinello-Rahman pressure coupling [37, 38] of 1 bar, with a coupling constant of τ=1 ps. A cutoff of 1.2 nm was used for van der Waals interactions. Electrostatic interactions were computed using the PME algorithm [39], with a 1.2 nm cutoff for the direct space calculation. The simulations contain approximately ~100 DMPC lipids and ~3600 water molecules in FLEXSPC model [29]. The total number of atoms was ~17000. The number of atoms is not the identical for all systems due to the different instances of lipids and water removed in each bilayer insertion process, the protonation state, the crystal water in the X-ray structure and the different number of amino acids in each of the initial experimentally-solved structures.

Analysis

The simulations were visualized and analyzed with the Visual Molecular Dynamics (VMD) program [40]. The pore radius profile during the simulation was computed at 100 ps intervals using the program HOLE [41, 42].

Results

The aim of this study was to comparatively investigate three different experimentally derived structures for the M2 H^+ channel using MD simulations. Below we report our results studying the protein stability, maintenance of secondary structure, water connectivity and conductivity and other parameters on each of the structures individually.

Stability

Several measures were employed in order to gauge the stability of the different structures. First, deviation from the original structures is discussed, followed by analysis of secondary structure. Second, the tilt angles of the helices, and an analysis of both native contacts and total number of contacts are presented. We define native contacts as contacts between non-bonded atoms, Cα or side-chains, that are located 3 amino acids apart in the primary sequence and are spatially close. It can be used to determine the deviation from the "native" experimental structure during the simulation. For our analysis, we have used a spatial cutoff of 7 Å. The native contacts were measured for two groups: (1) between the Cα atoms only and (2) between the side-chain atoms only. In addition, the total amount of contacts in each structure was counted throughout each of the simulations in order to examine the stability of the system. An ever-changing number of contacts between different residues of a protein means that the 3D structure itself is also changing and unstable. A decrease in the amount of contacts would mean the helical bundle is less compact and that the pore is wider. The contacts that were counted here, are Cα contacts in radius of $\leq$7Å, excluding contacts of bonded atoms within a range of 3 helical residues.

X-Ray structure

All simulations, irrespective of protonation state diverged from the initial structure by a Cα-RMSD of 1.8–2.5Å. As presented in Fig. 2, the neutral channel, without any protonated histidines has converged after ~4.5 ns of simulation. The symmetric bi-protonated channel had converged from 3–7 ns and on, while the tri-protonated channel had converged approximately after 5 ns. Moreover, the triply protonated channel seems to have diverged the

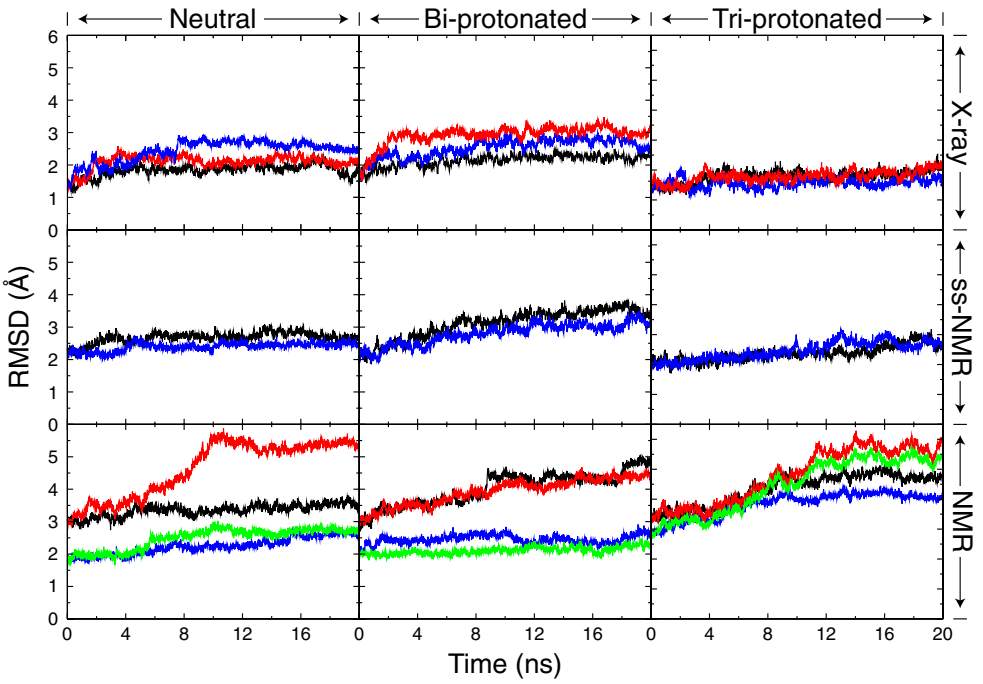

Fig. 2 RMSD for Cα atoms from 20 ns simulations of M2 according to the initial three structures under different histidine protonation state. Top row: X-ray structure (pdb: 3BKD). Middle row: solid state NMR-based structure (pdb: 1NYJ). Bottom row: solution NMR structure (pdb: 2RLF). Left column: neutral channel (0 protons). Middle column: bi-protonated channel (2 protons). Right column: tri-protonated channel (3 protons). The different colors represent different trajectories, each represent an independent unbiased trial. The only exception is the solution NMR structure, where black and red represent RMSD of the whole protein (independent trials), while the blue and green represent RMSD of the TM region only, for the same trials, respectively

least amount from the original structure, the relevance of which will be elaborated below.

The helix retention of the pores varied between 75–80 % as shown in Fig. 3. The neutral channel remained stable on a 80 % helical retention during the simulations. The protonated channels sometime fluctuated around 75 %, but were relatively stable as well.

As depicted in Fig. 4, for the simulations deriving from the X-ray structure, the tilt angles mostly converged to a range of 30°–45°. This is relatively consistent with experimental measurements [21, 22].

The percentage of native contacts maintained is presented in Fig. 5. For the Cα atoms, 82–95% of the native contacts were maintained in all simulations, where the tri-protonated state maintained the highest number of native contacts (90–95%), the bi-protonated state maintained a little less, and finally the neutral state maintained 82–90% of the contacts. For the side-chain atoms, the percentage of

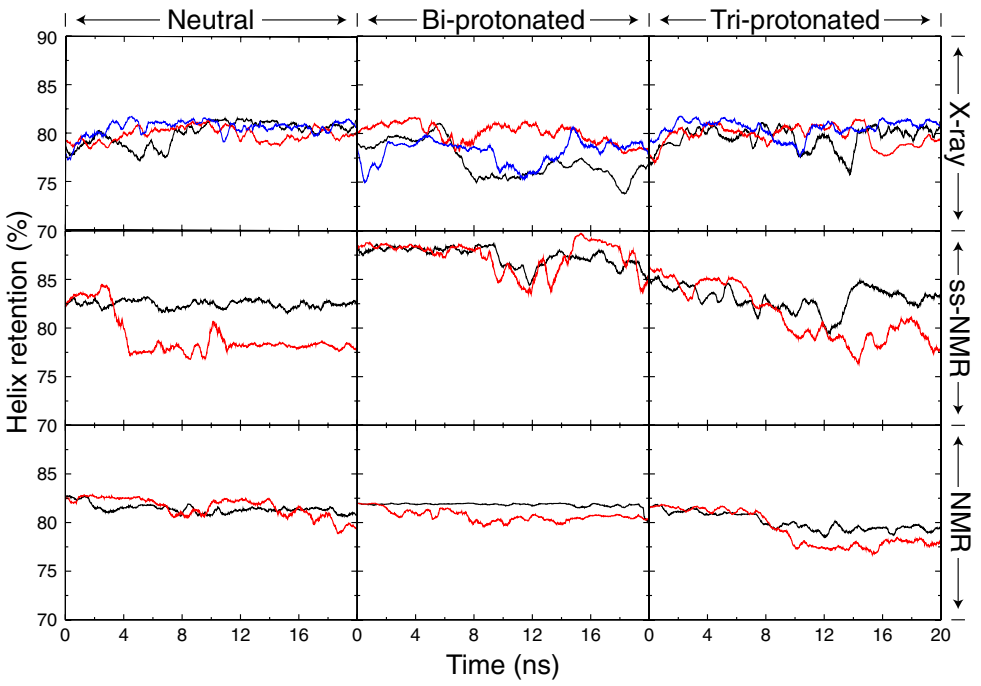

Fig. 3 Helix retention from 20 ns simulations of M2 according to the initial three structures under different histidine protonation state. Top row: X-ray structure (pdb: 3BKD). Middle row: solid state NMR-based structure (pdb: 1NYJ). Bottom row: solution NMR structure (pdb: 2RLF). Left column: neutral channel (0 protons). Middle column: bi-protonated channel (2 protons). Right column: tri-protonated channel (3 protons). The different colors represent different trajectories, each represent an independent unbiased trial

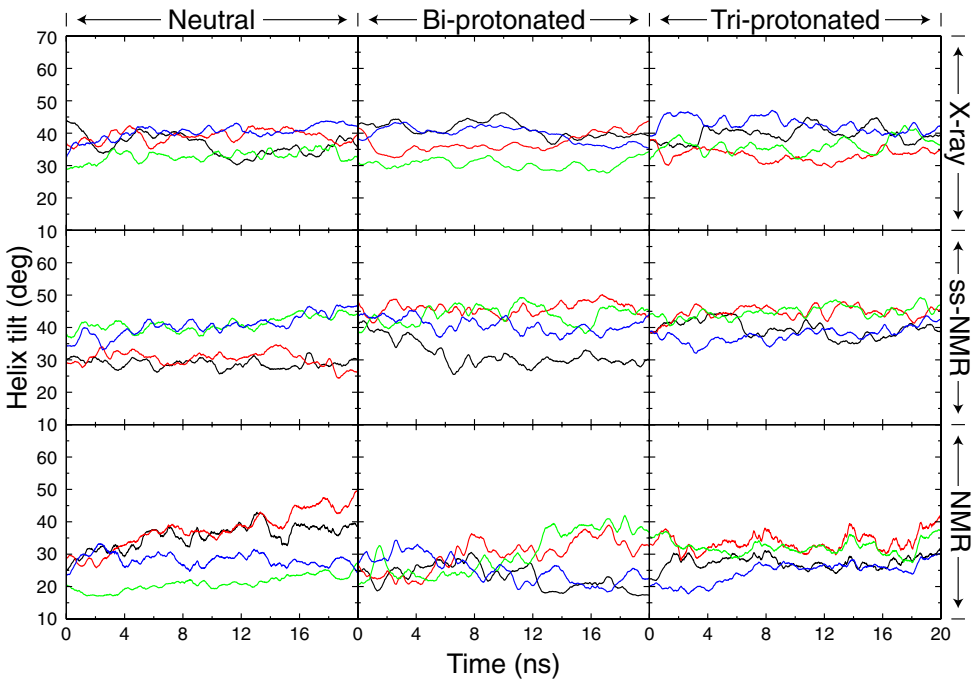

Fig. 4 Helix tilts for 20 ns simulation of M2 according to the initial three structures under different histidine protonation state. Top row: X-ray structure (pdb: 3BKD). Middle row: solid state NMR-based structure (pdb: 1NYJ). Bottom row: solution NMR structure (pdb: 2RLF). Left column: neutral channel (0 protons). Middle column: bi-protonated channel (2 protons). Right column: tri-protonated channel (3 protons). The different colors represent individual helices

native contacts maintained were 68–75% for the tri-protonated state, 65–73% for the bi-protonated state, and 60–73% for the neutral state.

As for the total number of contacts, we have found that it was stable during the simulation and that it correlated to the water connectivity of the channel. As depicted in Fig. 6, the X-ray structure exhibited a relatively stable number of contacts that can be divided into two. A high number of contacts corresponding to a non-conductive pore, for the neutral, tri-protonated, and two out of three trials of the bi-protonated. A slightly lower number of contacts, representing a partially conductive pore, for the third trial of the bi-protonated channel.

Solid state NMR-based model

The structures obtained during the simulations diverged from the original structure by 2.5–3.75 Å. The neutral

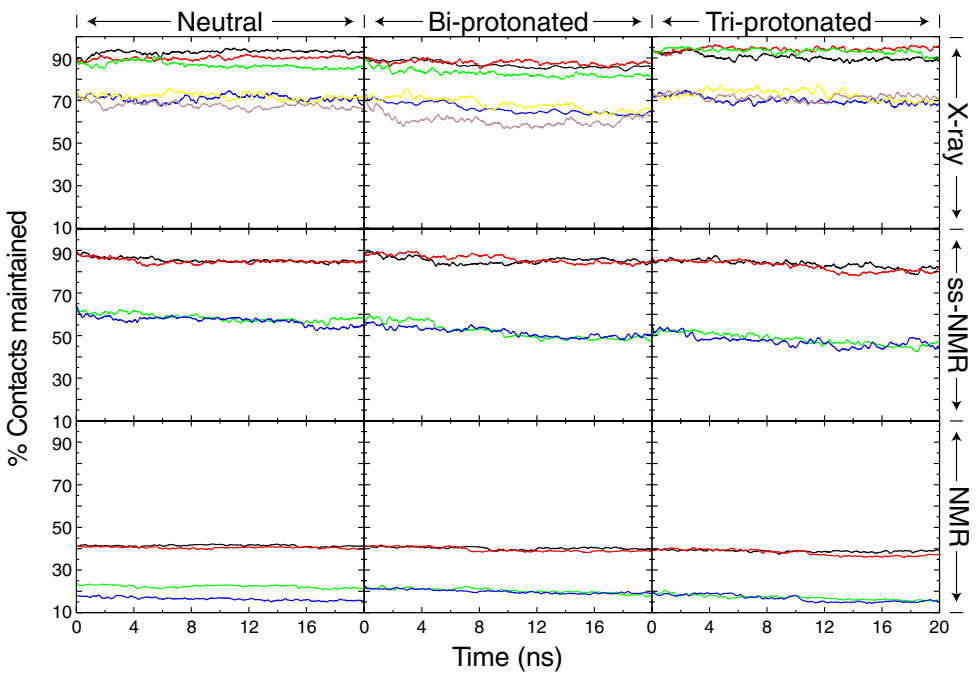

Fig. 5 Retention of native contacts for 20 ns simulation of M2 according to the initial three structures under different histidine protonation state. Top row: X-ray structure (pdb: 3BKD). Middle row: solid state NMR-based structure (pdb: 1NYJ). Bottom row: solution NMR structure (pdb: 2RLF). Left column: neutral channel (0 protons). Middle column: bi-protonated channel (2 protons). Right column: tri-protonated channel (3 protons). The different colors represent different trajectories, each represent an independent unbiased trial

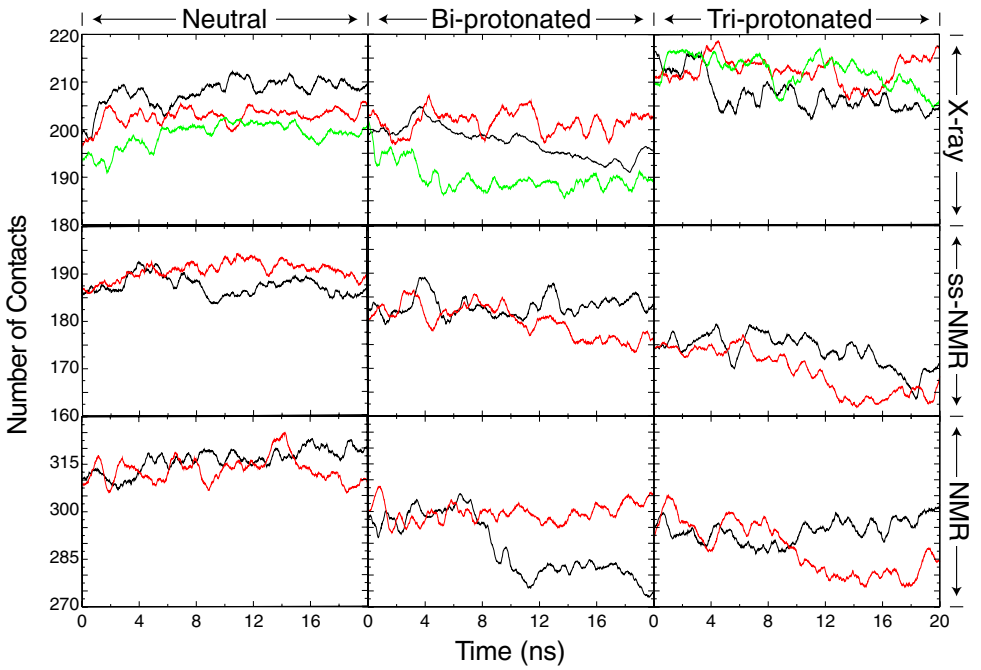

Fig. 6 Analysis of total number of contacts for 20 ns simulation of M2 according to the initial three structures under different histidine protonation state. Top row: X-ray structure (pdb: 3BKD). Middle row: solid state NMR-based structure (pdb: 1NYJ). Bottom row: solution NMR structure (pdb: 2RLF). Left column: neutral channel (0 protons). Middle column: bi-protonated channel (2 protons). Right column: tri-protonated channel (3 protons). The different colors represent different trajectories, each represent an independent unbiased trial

channel had converged after 5 ns of simulation to a structure that was distinct from the starting configuration by a Cα-RMSD of 2.5–3 Å. The symmetric bi-protonated channel had converged after 8–10 ns to an RMSD of 3–3.75 Å while the tri-protonated channel had diverged from the initial structure slowly, converging approximately at 12 ns around 2.3–2.7 Å (see Fig. 2).

The helix retention of the pores varied between 77–83 % for the neutral channel, 85–90 % for the bi-protonated channel, and 79–83 % for the triply protonated channel (see Fig. 3).

For simulations derived from the solid state NMR-based structure, the tilt angles viewed during the simulations mostly ranged from 30°–50° for the neutral and triply protonated channels. However, the bi-protonated channel seemed to have helices with unstable tilt angles, ranging from 25°–60° (see Fig. 4).

The native Cα contacts maintained in these simulations were 80–90%, where the tri-protonated state was the least stable of all (80–85%), and the rest of the simulations started around 90% and descended to 85%. The side-chain contacts were lower as well, as shown in Fig. 5, between 45-65%.

The total number of contacts, for the neutral, non conductive, channel has a rather consistent number of 185–190 contacts. This number only decreased for the other protonation states, when the histidines were charged. As noted below, the bi-protonated channel simulations resulted in one partially open channel and one fully open channel. These data correlate to the number of contacts, as shown in Fig. 6. For the partially open channel, the number of contacts decreased to 180–185 in total. For the fully open channel, the number of contacts can be seen descending during the simulation to 175 contacts in total. The triply protonated channel which was fully open, has an even lower number of contacts, fluctuating between 160–170 contacts in total.

Solution NMR-based model

The simulations of this structure had diverged the most from the original structure. However, when measuring the RMSD for the transmembrane segment alone, the neutral and bi-protonated channels were quite stable, almost like the X-ray structure. The neutral channel had diverged by 3.5 Å within 3 ns before stabilizing for one trial, and 5.3 Å within 10 ns in another trial. However, when examining the TM region only, both trials had converged on an RMSD of 2.7 Å. The bi-protonated channel had diverged by 4.3–4.8 Å from the initial structure, while the structures did not converge completely. The first bi-protonated trial consisted of a several temporarily stable phases with sharp transitions in between, while the second trial diverged from the initial structure slowly. Again, the transmembrane regions had shown a more stable structure, converging on 2.3 Å and 2.5 Å. The triply protonated channel had a Cα RMSD of 4.7 Å from the initial structure for one trial and 6 Å for another. Convergence had occurred between 7 ns to 13 ns of the simulation (see Fig. 2). Unlike the previous protonation state, this time the conformation of the TM region alone converged to a high RMSD for both trials. This may occur due to the initial channel's radius, which is narrower than the other experimental structures. Low pH, in which three histidines are protonated, could cause a high steric repulsion and a disruption of the entire structure.

The helix retention of the protein was calculated for the TM region only. The helices maintained their helicality just as well as the previous structures. For the neutral channel, the helix retention was approximately 78–83 %, for the bi-protonated channel: 80–82 % and for the triply protonated channel it fluctuated between 74–82 %.

A wider range of average tilt angles was viewed during the simulations of the solution NMR-based model. Figure 4 shows that these angles ranged between 20°–60°. The largest spread of tilt values was observed in the tri-protonated channel.

The amount of native contacts maintained during the simulations of this structure were significantly lower than any of the others. Only 40–42 % of the Cα contacts were maintained, while 18–23 % of the side-chain contacts were maintained. It should be noted that approximately 60 % of the native contacts were lost in the equilibration phase, during the positional restraints process (data not shown).

An analysis of the total number of contacts reveals that the neutral channel contains 305–325 contacts. The bi-protonated channel shows a similar tendency as for the ssNMR analysis, where the more conductive channel has a significant decrease in the number of contacts (270–280), while the less conductive, yet still partially open channel, has a stable number of contacts (~300). The tri-protonated channel presents an opposite correlation, where the least conductive channel converges to a lower number of contacts ranging around 280, while the trial that formed a channel that is open ~25 % of the simulation time, converges to 300 contacts. This could be due to a disruption in the structure, as one of the helices is pulled away by its C-terminal, and causes the pore to close on the N-terminal.

Water connectivity, diffusive permeability and pore radius

According to the Grotthus mechanism, proton transport does not occur as transport of a single proton molecule through solution, but as a net result of many formation breaking of covalent bonds between the proton and adjacent water molecules. In order to examine the permeability of the M2 H^+ channel in each of the different systems, the pore behavior was examined in terms of water connectivity and diffusive permeability.

Specifically, two measurements regarding the pore properties were undertaken. First, water connectivity, measured the formation of a water-wire throughout the pore, at maximum distances of 3.5 Å between adjacent water molecules. The second analysis measured the diffusive water permeability inside the pore, that is, a measure of the number of water molecules that traversed the pore from one side of the bilayer to the other, in the absence of net flux. Finally, the pore radius profile during the simulations was computed at 100 ps intervals, a representative profile is shown for each set of trials.

X-Ray structure

As depicted in Table 2, the X-ray structure rarely exhibits a continuous water wire throughout the duration of the simulations: the neutral channel is always blocked. The bi-protonated channel is nearly always blocked in 2 out of 3 trials (a water wire is formed less than 1 % of the time). However, the third trial contains a continuous water wire during ~27 % of the simulation time. As for the Tri-protonated channel, all trials present a blocked channel according to the criteria of water wire. However, at a 4.5 Å distance, the channel is open 1 % of the simulation time (data not shown).

In addition, the number of incidents in which a whole water molecule traversed the pore was measured. Table 3 shows that all trials but one exhibited few such incidents (0–5). The only exception is the simulation that presented a continuous water wire 27 % of the simulation time. It contained 46 incidents of whole water molecules passing throughout the pore.

The pore radius profile presents only a single location in which the X-ray structure is blocked (see Fig. 7). This location corresponds to Val-27 and continues to be narrow (<1.25 Å) in different protonation states. Looking down from Val-27 towards the C-terminal, the pore becomes wider, though a slight decrease in the radius is observed near the histidines, though the pore is still wide open (radius of 3–3.5 Å). Another slight blockage is found in at the N-terminal serine and aspartic acid, on one trial of the neutral channel and in the tri-protonated channel.

Solid state NMR-based model

Examining the water passage in the simulation based on the ssNMR model, revealed a similar behavior as shown

Table 2 Analysis of water wire formation (connectivity) throughout each simulation generated from each structure

Structure	0-H	2-Hs	3-H
X-ray trial 1	0.15 %	0.2 %	0 %
X-ray trial 2	0 %	0.4 %	0 %
X-ray trial 3	0 %	27.39 %	0 %
ssNMR trial 1	0.35 %	19.69 %	95.75 %
ssNMR trial 2	5.85 %	95.75 %	99.95 %
solNMR trial 1	0 %	83.86 %	24.24 %
solNMR trial 2	0 %	24.59 %	4.05 %

The terms 0-H, 2-Hs, 3-H refer to the protonation state of M2: neutral, symmetrically bi-protonated, and tri-protonated.

Table 3 Water conductivity in the pore throughout each simulation generated from each structure

Structure	0-H	2-Hs	3-H
X-ray trial 1	0	4	4
X-ray trial 2	0	2	0
X-ray trial 3	0	46	3
ssNMR trial 1	0	4	99
ssNMR trial 2	0	174	62
solNMR trial 1	0	32	2
solNMR trial 2	0	7	3

The terms 0-H, 2-Hs, 3-H refer to the protonation state of M2: neutral, symmetrically bi-protonated, and tri-protonated.

previously by [24]. Table 2 shows a formation of a water wire up to 6 % of the simulation time for the neutral channel. However, this is observed only throughout the first 0.5 ns of the simulation, during equilibration time. Thus, the neutral channel is always blocked during the production time of the simulation. The bi-protonated channel formed a partially open pore (a water wire exists for 20 % of the simulation) in one trial, or a permanently open pore (95 % of the simulation) in the second trial. The triply protonated channel formed a permanently open channel over 95 % of the time in both trials.

As for water conductivity, the neutral channel presented no water passage at all, while the protonated channels usually show a large number of incidents of water passage (see Table 3).

In contrast to the X-ray structure, the pore radius profile of this structure does show a correlation to the protonation states of the channel. The neutral channel is blocked at His-37 and Trp-41; however, the other states render the pore wider at this location with a radius that is larger than 2 Å.

Solution NMR-based model

According to the water-wire criteria, the neutral channel was always blocked. The bi-protonated channels exhibited a similar water connectivity to the ssNMR model. That is, one trial produced a partially opened channel with a formation of a water wire 24 % of the simulation time, and the second trial exhibited a formation of a water wire throughout a much larger portion of the time (~83 %). This is also seen in the differences of the water conductance results (Table 3). The triply protonated channel formed a partially open pores for 4 % and 24 % of the simulation time. However, the tri-protonated channels only produced few incidents of an entire water molecule conductance.

The pore radius profile of this structure was entirely different than the others. The Solution-NMR model is very narrow (≤1.5 Å) at a few positions along the pore, making it almost completely blocked in the space between Val-27 to His-37 and Trp-41 in the neutral state, after 5 ns of simulation. The bi-protonated state shows a wider pore, although two obvious bottlenecks remain: Val-27 and Trp-41. These bottlenecks are more obvious in the second trial of the bi-protonated state, where the channel is more constricted and exhibits less instances of a continuous water wire. The tri-protonated state presents a larger repulsion between the histidines, so that the constriction of the pore remains mainly between Val-27 to Ile-33. The first trial also presents another constriction near Trp-41 (data not shown).

Discussion

This study attempted to present a comprehensive comparison using MD simulations of the newly emerging structures of the M2 protein. Exploring the dynamics, stability and interactions of these structures over time instead of one snapshot may account for the manifold possible range of orientations that M2 may explore.

The structures differed, not only in the methodology that was used to determine them, but also in several key aspects: pH, lipid bilayer versus detergent, hydration level, length of peptide, and presence of an inhibitor. Therefore, these structures were compared in a uniform environment, in several different protonation states that are believed to correlate to open and closed channels [30].

The results show that the X-ray structure is the most stable one over 20 ns, for all three protonation states. The ssNMR structure was also quite stable during the simulation although on average, it moved further away from the initial structure. The solution NMR structure RMSD of the transmembrane region was as stable as the X-ray structure for a closed (neutral) and open (bi-protonated) states, but it has diverged from the initial structure very much for the tri-protonated state. The extra C-terminal in the solution NMR structure had significantly diverged much in all simulations. It could be that the aqueous C-terminal is too short to keep in a stable formation in water while separated from the rest of the C-terminal of the protein which should have restricted its movement.

For all of the above structures, the lipid bilayer maintains its arrangement around the protein, such that despite random fluctuations, it keeps a relatively constant distance from the protein's center of mass (data not shown). The lipid hydrophobic core accommodates the hydrophobic core of the channel, while the polar lipid headgroups interact with the polar and charged residues at the channel edges. The only polar residues in the channel which do not interact with the lipid headgroups are Ser-31 and His-37.

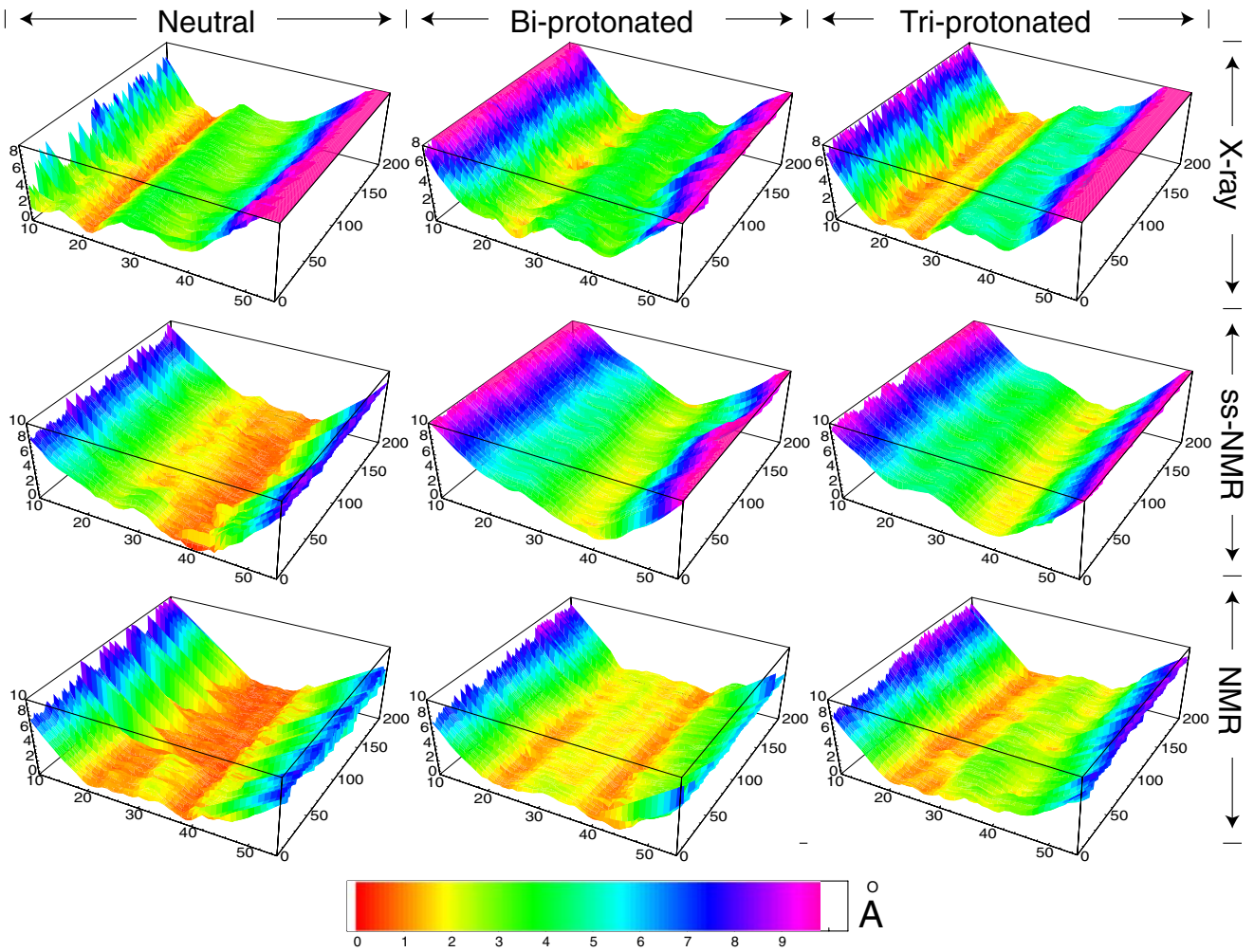

Fig. 7 Pore radius profile for 20 ns simulation of M2 according to the initial three structures under different histidine protonation state. Top row: X-ray structure (pdb: 3BKD). Middle row: solid state NMR-based structure (pdb: 1NYJ). Bottom row: solution NMR structure (pdb: 2RLF). Left column: neutral channel (0 protons). Middle column: bi-protonated channel (2 protons). Right column: tri-protonated channel (3 protons)

However, these residues can interact with the water molecules that solvate the pore itself.

An analysis of the amount of native contacts maintained during the simulation has shown that the X-ray structure orientations that were explored, deviate less than all other structures, maintaining the highest amount of Cα contacts for the tri-protonated channel, and a little less for the other protonation states. It also maintained the highest amount of side-chain contacts out of all structures. The ssNMR structure simulations were also relatively close to the original structure in terms of native contacts, and the solution NMR structure simulations presented the least preservation of the native contacts recorded in the original PDB structure.

In addition the analysis of single-helix tilt angle variations during the simulations had shown that the X-ray structure had the least divergence of tilt, varying approximately between 30–45°, close to the experimentally measured values [21, 22]. The ssNMR structure had a slightly larger divergence between 25–45°, which occurred mainly in the neutral and bi-protonated channels, however, it was still in agreement with previous simulations [19]. The solution NMR structure had the most fluctuative tilt angles, varying between 20–50° for the neutral and bi-protonated states. It is interesting to note that all structure seem to fluctuate the least in their tri-protonated state.

Surprisingly, the helicality of the pore helices maintained during the simulations was quite similar for all structures, where the NMR structures usually maintained over 80% helicality (and nearly 90% for the bi-protonated ssNMR simulations), and the X-ray structure maintained a slightly lower range of helicality (75%–80%).

A comparison of the water conductivity and water-wire formation has shown that the X-ray structure is closed for

the neutral state, nearly closed for the tri-protonated state and partially open for the bi-protonated state. Thus, our simulations do not present a clear picture of how the channel changes as a function of the charging of the histidines. It seems that the histidines are too far apart, that charging them does not cause a repulsion effect that opens the pore. However one must note that water conductivity and not H^+ conductivity was analyzed in this study and the fact that water does not permeate through the channel does not preclude H^+.

As stated in a previous study [26], the pore is almost completely constricted near its entry at Val-27. One possible explanation to the negligible effect of the His-37 on gating, is that due to the truncated cone shape of the pore, the repulsion of the histidines on the C-terminal causes the N-terminal side to move closer in a scissor-like form, closing the Val-27 gate. The simulations of the X-ray structure indeed show that the channel stays constricted most of the time due to Val-27, and that there is a correlation between the formation of a water-wire and the growing distances between the side-chains of Val-27 (data not shown). Moreover, one must recognize that any rearrangement following protonation may take longer than the duration of the simulation.

In the bi-protonated form, one trial out of three had exhibited a partially open pore. The difference between the trials stems from different initial velocities given to the atoms in each trial which can lead to slightly different dynamics for the whole structure. Nonetheless, the entire 60 ns of simulation time for the bi-protonated X-ray structure should be regarded as a whole and therefore it is possible to say there is an equilibrium between an open and closed states in the bi-protonated form of the X-ray structure. However, when three histidines are charged, the repulsion between them could be too high, that a scissor-like movement may causes Val-27 to be closed the entire time. These data agree with the low conductivity of the channel that was measured experimentally [10, 11].

In contradiction to the X-ray structure, the conductivity and formation of a water-wire in the simulations derived from ssNMR based structures, did not correlate to Val-27. Rather, they presented a strong correlation to the His-37 protonation states, and to the distances between His-37 side-chains. Similar studies in the past have also indicated that the primary pore region that limits proton conductivity is the region of the histidines [19, 23, 24]. In our study, the channel was entirely closed when no histidine was charged, but nearly completely open when 2 or 3 histidines were charged, a surprising result given that M2 was shown to be a channel with slow ion conduction rate [10, 11].

A recent study by Chen et al. [25], obtained a low frequency of water-wire occurrences even for a tri-protonated channel. However, this study had used an earlier structure (PDB code 1MP6), reconstructed from one monomer, with a slightly different tilt angle. In addition, a shorter simulation time and different cutoffs were used for the estimation of water-wire occurrences. Overall, these observations may lead to a conclusion that the ssNMR structure of the entire tetramer complex deviates from the native structure of M2, although the model of one helix is similar.

The solution NMR structure presented correlation to the histidines as well, though not entirely. It exhibited a closed pore for the neutral state, and a partially conductive pore when 2 or 3 histidines were protonated. Since there was no obvious correlation to neither the distances between Val-27 nor His-37, it was unclear which other factors affect the conductivity of this structure. It could be that a combination of Trp-41, Val-27 and His-37 controls the conductance in this case [26, 27, 43].

In conclusion, three experimental structures of the M2 proton channel were subjected to extensive MD simulations. Different characteristics of the channel were explored over time. The X-ray structure was observed to be the most stable during these simulations, mainly in its tri-protonated form. The solution NMR structure was the least stable. The water conductance analysis had rendered the X-ray pore as nearly always blocked by Val-27. Despite that, it could be that the channel is open when two histidines are charged, as shown by the partial conductivity in its bi-protonated state. The ssNMR was nearly conductive (i.e., contains a continuous water wire) at all times when the histidines were protonated, blocked only when the channel was neutral, suggesting that this model might divert from the real structure of M2 in nature as very low conductance rates were measured for M2 in practice.

Acknowledgments This work was supported in part by grants from the Israeli science foundation (784/01,1249/05,1581/08) to ITA. ITA is the Arthur Lejwa Professor of Structural Biochemistry at the Hebrew University of Jerusalem. Molecular figures were generated using VMD.

References

1. Pinto LH, Holsinger LJ, Lamb RA (1992) Influenza virus M2 protein has ion channel activity. Cell 69:517–528
2. Sakaguchi T, Tu Q, Pinto LH, Lamb RA (1997) The active oligomeric state of the minimalistic influenza virus M2 ion channel is a tetramer. Proc Natl Acad Sci USA 94:5000–5005
3. Hay AJ, Wolstenholme AJ, Skehel JJ, Smith MH (1985) The molecular basis of the specific anti-influenza action of amantadine. EMBO J 4:3021–3024
4. Hay AJ, Kennedy NC, Skehel JJ, Appleyard G (1979) The matrix protein gene determines amantadine-sensitivity of influenza viruses. J Gen Virol 42:189–191
5. Duff KC, Gilchrist PJ, Saxena AM, Bradshaw JP (1994) Neutron diffraction reveals the site of amantadine blockade in the influenza A M2 ion channel. Virology 202:287–293

6. Wang C, Lamb RA, Pinto LH (1995) Activation of the M2 ion channel of influenza virus: a role for the transmembrane domain histidine residue. Biophys J 69:1363–1371
7. Mould JA, Drury JE, Frings SM, Kaupp UB, Pekosz A, Lamb RA, Pinto LH (2000) Permeation and activation of the M2 ion channel of influenza A virus. J Biol Chem 275(31):038–50
8. Shimbo K, Brassard DL, Lamb RA, Pinto LH (1996) Ion selectivity and activation of the M2 ion channel of influenza virus. Biophys J 70:1335–1346
9. Chizhmakov IV, Geraghty FM, Ogden DC, Hayhurst A, Antoniou M, Hay AJ (1996) Selective proton permeability and pH regulation of the influenza virus M2 channel expressed in mouse erythroleukaemia cells. J Physiol 494:329–336
10. Lin TI, Schroeder C (2001) Definitive assignment of proton selectivity and attoampere unitary current to the M2 ion channel protein of influenza A virus. J Virol 75:3647–3656
11. Vijayvergiya V, Wilson R, Chorak A, Gao PF, Cross TA, Busath DD (2004) Proton conductance of influenza virus M2 protein in planar lipid bilayers. Biophys J 87:1697–1704
12. Sansom MS, Kerr ID, Smith GR, Son HS (1997) The influenza A virus M2 channel: a molecular modeling and simulation study. Virology 233:163–173
13. Brewer ML, Schmitt UW, Voth GA (2001) The formation and dynamics of proton wires in channel environments. Biophys J 80:1691–1702
14. Lear JD (2003) Proton conduction through the M2 protein of the influenza A virus; a quantitative, mechanistic analysis of experimental data. FEBS Lett 552:17–22
15. Pinto LH, Dieckmann GR, Gandhi CS, Papworth CG, Braman J, Shaughnessy MA, Lear JD, Lamb RA, DeGrado WF (1997) A functionally defined model for the M2 proton channel of influenza A virus suggests a mechanism for its ion selectivity. Proc Natl Acad Sci USA 94(11):301–306
16. Forrest LR, Tieleman DP, Sansom MS (1999) Defining the transmembrane helix of M2 protein from influenza A by molecular dynamics simulations in a lipid bilayer. Biophys J 76:1886–1896
17. Sansom MS, Tieleman DP, Forrest LR, Berendsen HJ (1998) Molecular dynamics simulations of membranes with embedded proteins and peptides: porin, alamethicin and influenza virus M2. Biochem Soc Trans 26:438–443
18. Husslein T, Moore PB, Zhong Q, Newns DM, Pattnaik PC, Klein ML (1998) Molecular dynamics simulation of a hydrated diphytanol phosphatidylcholine lipid bilayer containing an alpha-helical bundle of four transmembrane domains of the influenza A virus M2 protein. Faraday Discuss 111:201–208
19. Smondyrev AM, Voth GA (2002) Molecular dynamics simulation of proton transport through the influenza A virus M2 channel. Biophys J 83:1987–1996
20. Nishimura K, Kim S, Zhang L, Cross TA (2002) The closed state of a H^+ channel helical bundle combining precise orientational and distance restraints from solid state NMR. Biochemistry 41 (13):170–177
21. Kovacs FA, Cross TA (1997) Transmembrane four-helix bundle of influenza A M2 protein channel: structural implications from helix tilt and orientation. Biophys J 73:2511–2517
22. Kukol A, Adams PD, Rice LM, Brunger AT, AT I (1999) Experimentally based orientational refinement of membrane protein models: A structure for the Influenza A M2 H^+ channel. J Mol Biol 286:951–962
23. Wu Y, Voth GA (2005) A computational study of the closed and open states of the influenza a M2 proton channel. Biophys J 89:2402–2411
24. Kass I, Arkin IT (2005) How pH opens a H^+ channel: the gating mechanism of influenza A M2. Structure 13:1789–1798
25. Chen H, Wu Y, Voth GA (2007) Proton transport behavior through the influenza A M2 channel: insights from molecular simulation. Biophys J 93:3470–3479
26. Stouffer AL, Acharya R, Salom D, Levine AS, Di Costanzo L, Soto CS, Tereshko V, Nanda V, Stayrook S, DeGrado WF (2008) Structural basis for the function and inhibition of an influenza virus proton channel. Nature 451:596–599
27. Schnell JR, Chou JJ (2008) Structure and mechanism of the M2 proton channel of influenza A virus. Nature 451:591–595
28. Wang JF, Kim S, Kovacs F, Cross TA (2001) Structure of the transmembrane region of the M2 protein H^+ channel. Protein Sci 10:2241–2250
29. Berendsen HJC, Grigera JR, Straatsma TP (1987) The missing term in effective pair potentials. J Phys Chem 91:6269–6271
30. Hu J, Fu R, Nishimura K, Zhang L, Zhou HX, Busath DD, Vijayvergiya V, Cross TA (2006) Histidines, heart of the hydrogen ion channel from influenza A virus: toward an understanding of conductance and proton selectivity. Proc Natl Acad Sci USA 103:6865–6870
31. Lindahl E, Hess B, van der Spoel D (2001) GROMACS 3.0: A package for molecular simulation and trajectory analysis. J Mol Mod 7:306–317
32. Hermans J, Berendsen HJC, van Gunsteren WF, PJP M (1984) A consistent empirical potential for water-protein interactions. Biopolymers 23:1513–1518
33. Berger O, Edholm O, Jahnig F (1997) Molecular dynamics simulations of a fluid bilayer of dipalmitoylphosphatidylcholine at full hydration, constant pressure, and constant temperature. Biophys J 72:2002–2013
34. Hess B, Bekker H, Berendsen HJC, Fraaije JGEM (1997) LINCS: A linear constraint solver for molecular simulations. J Comp Chem 18:1463–1472
35. Nóse S (1984) A molecular dynamics method for simulations in the canonical ensemble. Mol Phys 52:255–268
36. Hoover WG (1985) Canonical dynamics - equilibrium phase-space distributions. Phys Rev A 31:1695–1697
37. Parrinello M, Rahman A (1981) Polymorphic transitions in single crystals: A new molecular dynamics method. J Appl Phys 52:7182–7190
38. Nóse S, Klein ML (1983) Constant pressure molecular dynamics for molecular systems. Mol Phys 50:1055–1076
39. Darden T, York D, Pedersen L (1993) Particle mesh Ewald: An N-log(N) method for Ewald sums in large systems. J Chem Phys 98 (10):089–92
40. Humphrey W, Dalke A, Schulten K (1996) VMD–Visual Molecular Dynamics. J Mol Graphics 14:33–38
41. Smart OS, Neduvelil JG, Wang X, Wallace BA, Sansom MS (1996) HOLE: a program for the analysis of the pore dimensions of ion channel structural models. J Mol Graphics 14:354–360
42. Smart OS, Breed J, Smith GR, Sansom MS (1997) A novel method for structure-based prediction of ion channel conductance properties. Biophys J 72:1109–1126
43. Tang Y, Zaitseva F, Lamb RA, Pinto LH (2002) The gate of the influenza virus M2 proton channel is formed by a single tryptophan residue. J Biol Chem 277(39):880–886